Adhesion Forces of Lipids in a Phospholipid Membrane Studied by Molecular Dynamics Simulations

Siewert-Jan Marrink,* Oliver Berger,* Peter Tieleman,# and Fritz Jähnig*
*Max-Planck-Institut für Biologie, Abteilung Membranbiochemie, Tübingen, Germany, and #University of Groningen, Department of Biophysical Chemistry, Groningen, The Netherlands

ABSTRACT Lipid adhesion forces can be measured using several experimental techniques, but none of these techniques provide insight on the atomic level. Therefore, we performed extensive nonequilibrium molecular dynamics simulations of a phospholipid membrane in the liquid-crystalline phase out of which individual lipid molecules were pulled. In our method, as an idealization of the experimental setups, we have simply attached a harmonic spring to one of the lipid headgroup atoms. Upon retraction of the spring, the force needed to drag the lipid out of the membrane is recorded. By simulating different retraction rates, we were able to investigate the high pull rate part of the dynamical spectrum of lipid adhesion forces. We find that the adhesion force increases along the unbinding path, until the point of rupture is reached. The maximum value of the adhesion force, the rupture force, decreases as the pull rate becomes slower, and eventually enters a friction-dominated regime. The computed bond lengths depend on the rate of rupture, and show some scatter due to the nonequilibrium nature of the experiment. On average, the bond length increases from ~1.7 nm to 2.3 nm as the rates go down. Conformational analyses elucidate the detailed mechanism of lipid-membrane bond rupture. We present results of over 15 ns of membrane simulations. Implications for the interpretation and understanding of experimental rupture data are discussed.

INTRODUCTION

The typical binding free energy of a phospholipid in a membrane is about 80–100 kJ/mol as estimated from critical micelle concentration (CMC) data (Cevc and Marsh, 1987). On a biological scale this is a huge energy, implying that under equilibrium conditions the lipids will have only a very small tendency to leave the membrane. However, many processes that involve membranes (e.g., cell binding, fusion, protein insertion) require deformations of the equilibrium membrane structure and at least a partial removal of lipids from the membrane. Therefore, an external force needs to be applied to drive lipids away from their equilibrium position in an activated process. Such an external force could arise from an ion gradient, from coupling to another process, or in general from any thermodynamic gradient. An important feature of such an activated process is that it occurs under nonequilibrium conditions, implying a breakdown of simple thermodynamics. Under nonequilibrium conditions, the end state is not determined by an equilibrium property as the free energy, but by the forces that drive the process away from the equilibrium path.

A biologically relevant example illustrating the difference between equilibrium and nonequilibrium pathways is the following. In cell-cell binding a typical bridge between the two cells may consist of a lipid-anchored protein at the one cell surface, ligated to a lipid-anchored substrate at the other cell surface. Let us assume a binding energy of 50 kJ/mol for the protein ligand complex, and a binding energy of 100 kJ/mol for the anchoring lipids. The question is: which bond ruptures upon retraction of the two cell surfaces? In an equilibrium situation, the chances of bond breaking are simply given by the Boltzmann factor of their binding free energies, in which case the protein-ligand would prove to be the weakest link. However, the chance of spontaneous dissociation of a 50 kJ/mol bond is fairly small, and in reality an external force will be used to unbind the cells, i.e., a nonequilibrium pathway is used. In that case, the bond rupture is determined by the slope of the binding free energy along the unbinding path rather than by the free energy difference. The bond with the smallest slope has the lowest strength, and is most likely to break. In the above example, when the strength of the receptor-ligand bond exceeds the cohesive force retaining the lipid anchor in the membrane, the lipid will be extracted under externally applied stress. Exactly this kind of behavior has been observed experimentally for a variety of protein-ligand complexes anchored by lipids in different cells (Leckband et al., 1994; Evans et al., 1991).

Bell first realized that the strength of bonds, and thus the force required to break them, depends on the slope of the binding free energy rather than on the free energy difference (Bell, 1978). The strength of adhesion bonds also depends on the rate at which a particular bond is being ruptured because of the nonequilibrium nature of the process. The faster the process, the more the nonequilibrium path will deviate from the equilibrium path. Moreover, frictious forces become important and may eventually constitute the dominant contribution to the total force. We therefore need to look at different time scales to study the binding forces of

Received for publication 11 August 1997 and in final form 31 October 1997.

Address reprint requests to Peter Tieleman, University of Groningen, Dept. of Biophysical Chemistry, Nijenborgh 4, 9747 AG Groningen, The Netherlands. Tel.: 31-503634338; Fax: 31-503634800; E-mail: P. Tieleman@chem.rug.nl.

In memory of Fritz Jähnig (1996).

0006-3495/98/02/931/13 $2.00

a variety of biological complexes. In this context, the term dynamical spectroscopy (DS) has been launched recently (Evans and Ritchie, 1997).

Various experimental techniques exist to study the spectrum of molecular bond strengths. The optical tweezer (OT) method and the biomembrane force probe (BFP) technique operate at the slowest time scale, milliseconds to seconds. Somewhat faster time scales (down till microseconds) are probed by the atomic force microscope (AFM) and by the surface force apparatus (SFA). Computer simulations can study the fastest time scale in the nanosecond regime. The first computer studies on bond strengths were reported recently by Grubmüller et al. (1996). Their molecular dynamics (MD) simulations of rupture of the biotin-streptavidin complex showed the molecular details of the unbinding pathway, and probed a time regime where the forces are dominated by friction.

Inspired by their study, in this work we investigate the adhesion forces of lipids in membranes. The (dynamical) strength of the lipid-membrane bond is of general interest to cell binding, fusion, and protein insertion as indicated above, and of special importance for the anchoring of proteins to a membrane. Single lipid molecules often serve as membrane anchors for proteins, for example Braun's lipoprotein, alkaline phosphatase, and many others (for a review see Sefton and Buss, 1987). Their functionality is directly related to the adhesion forces of lipids in the membrane. The cell seems to have a highly sophisticated tool to regulate this functionality; by varying the lipid composition and modulating the phase transition it can alter the adhesion properties of the lipids in the membrane. Also, in biotechnological applications, lipid anchors are increasingly used for stabilization of liposomes (for a review see Woodle and Lasic, 1992).

To elucidate the molecular details of the lipid-membrane bond-breaking, we apply the MD simulation technique. During the simulations, single lipid molecules are pulled out of the membrane at different rates by a harmonic spring. Analysis of the computed forces and the concomitant conformational changes of the lipids during the extraction process reveals a detailed picture of the rupture process, much more detailed than the ones available from experimental data.

In the next section we will give a short review of both the theoretical and experimental background of lipid adhesion forces. This is followed by a description of the methods of simulation of the lipid bilayer, and of the extraction of the lipids out of the membrane. Thereafter, the results are presented, which are then discussed in a more general context. Finally, the main conclusions are briefly summarized.

REVIEW

Theory of bond rupture

Consider a complex of a molecule bound to some substrate. The force that is required to separate the bound state into the unbound state, the adhesion force, F_{adh}, depends on the time scale at which we are looking through the rate of bond rupture, v_{rup}, and on the separation distance, R, along the unbinding path. It is elucidating to think of the adhesion force within the framework of Langevin dynamics. Within this framework, the total adhesion force can be expressed as an interplay between forces of three different origins, i.e., thermodynamic (F_{thd}), frictional (F_{fr}), and random (F_{rand}),

$$F_{adh}(v_{rup}, R) = F_{thd}(v_{rup}, R) + F_{fr}(v_{rup}, R) + F_{rand}(v_{rup}, R) \quad (1)$$

each of which may depend on both v_{rup} and R. (Note that Eq. 1 is only an approximation, as the total force cannot be exactly separated into constituent parts if cross-correlations between them exist.)

Integration of the adhesion force along the unbinding path results in the adhesion energy E_{adh}:

$$E_{adh}(v_{rup}) = \int_0^R F_{adh}(v_{rup}, R) \quad \delta R \quad (2)$$

The maximum observed adhesion force along the unbinding path is denoted as the rupture force, for it is the minimal force needed to rupture the bond. The point along the unbinding pathway at which the rupture force is observed also defines the bond length R_{rup}.

The thermodynamic component in Eq. 1 arises from the free energy barrier that exists along the unbinding pathway. In the limit of zero rupture rate, the unbinding path will be reversible, and a true thermodynamic force arises, i.e.,

$$F_{thd}(0, R) = \delta G(R)/\delta R \quad (3)$$

The adhesion energy in this case equals the excess free energy of the bound state with respect to the unbound state. With increasing rates, the path will become more and more irreversible, and the thermodynamic force no longer equals the true, or equilibrium, thermodynamic force, but rather the slope of the local potential energy landscape.

The frictious component originates from nonrandom collisions with neighboring (solvent) molecules, and is strongly dependent on rupture rate. At zero velocity, no friction will be experienced. For small rates, and ideal solutions, the friction depends linearly on the pull rate:

$$\delta F_{fr}(v_{rup}, R)/\delta v_{rup} = \xi(R) \quad (4)$$

where $\xi(R)$ denotes the friction coefficient of the (local) surrounding medium. Nonlinear effects could show up at higher rates or in non-ideal solutions.

The random component arises from random thermal motion. The average value of this component will add up to zero at infinite long time, but long-time correlations may constitute a significant nonrandom contribution at faster rates. The magnitude of the thermal fluctuations depends, in principle, on temperature only, not on the rate of bond rupture. However, at fast rupture rates, the environment of

the reaction coordinate can be heated up, and in this way increase the magnitude of the thermal fluctuations locally.

Although based on simplistic theoretical arguments, the interplay between the three components of the total adhesion force as outlined above already results in quite a complicated picture of the expected rate dependency. Making suitable assumptions it is, however, possible to distinguish between several regimes in which one of the component forces dominates the other as the rate of rupture increases:

1. Equilibrium Diffusion Regime: this regime is entered when the thermal forces are large enough to overcome the thermodynamic force. This can happen if either the thermodynamic barrier is small, or if the time scale of bond rupture is slow enough to sample such a rare process as spontaneous bond breaking. For, at infinite times, the thermal forces will disintegrate any bonded system. In this regime, one will measure no adhesion force, and the bond strength is zero.
2. Activated Diffusion Regime: at somewhat faster rates of bond rupture, when spontaneous dissociation is rather unlikely, one enters a regime where both thermodynamic and thermal forces modulate the adhesion force. The thermal component induces a diffusive kind of motion that will lower the adhesion force that would arise from the thermodynamic component only. Theoretical considerations predict a weak power law dependency of the adhesion force versus pull rate in this regime (Evans and Ritchie, 1997).
3. Drift Regime: at rates where random thermal forces play only a minor role, diffusive motion is replaced by drift motion. When frictious forces are still small, the adhesion force is dominated by the thermodynamic force. If the unbinding process occurs far from equilibrium, the thermodynamic force will be dominated by enthalpic forces along the chosen unbinding path. The rate dependency is hard to predict, as it will depend on the details of the potential energy landscape. However, if the unbinding pathway still resembles the equilibrium unbinding pathway, the rate dependency is expected to be logarithmic (Evans and Ritchie, 1997). In this case, the adhesion energy will be close to the free energy of the system.
4. Friction Regime: above a certain pulling rate, friction forces will start to dominate the total adhesion force. As long as the limit of ideal solutions is still applicable, one predicts a linear relationship between the adhesion force and the pulling rate in this regime (Eq. 4).
5. Far from equilibrium, at ever increasing rates, several effects may occur, whether or not simultaneously. One effect arises from entering a regime in which the friction will not behave linearly. Another effect is that the thermodynamic force will reach a maximum value, reflecting the steepest slope of the potential energy surface, and yet another is that local heating of the reaction coordinate may become important. Rate dependencies of bond strengths in these cases are hard to predict.

This outline of the different regimes where some effects dominate others provides us with a basic feeling of the diversity of the dynamical spectrum of biological bond strengths, and is helpful to understand the differences between the existing experimental and computational methods. The regimes that are probed by the experimental and computational techniques are discussed below.

Experiments on bond rupture

At present there exist four different methods to study bond rupture in biological systems: AFM, SFA, OT, and BFP. Each of these methods is still undergoing improvements: both the accuracy and the range of applications steadily grow. Due to the different time scales at which the experimental methods operate, each of them provides additional insights into the dynamical strength of biological bonds. For, as we have discussed above, the measured rupture forces strongly depend on the rate of bond rupture. (Note that experimental methods are only able to measure the maximum adhesion force along the unbinding pathway, i.e., the rupture force. Computer experiments, on the other hand, can probe the adhesion force along the full reaction path).

The slowest time regime is probed by the OT and the BFP methods, which both operate at the millisecond-to-second time scale. Bond rupture events studied by these methods are therefore sensitive to the thermal motion along the unbinding path, i.e., fall into time regime (2). [Note that on even longer time scales measurements of bond strengths become meaningless as one would observe spontaneous dissociation processes.] The SFA and AFM operate at somewhat faster time scales, around the millisecond range. Thermal motion becomes a less dominant factor, and for certain systems the probed time regime may shift toward regime (3).

The faster part of the dynamical force spectrum, down to the picosecond range, cannot be probed by the existing experimental methods; however, it can be studied by computer simulations. In the microsecond range mean field methods seem the most suitable, whereas the nano-to-picosecond range is available to full atomistic methods such as MD. Recently, Grubmüller et al. (1996) successfully compared MD simulations of the rupture of the biotin-streptavidin complex with an analogous AFM experiment (Florin et al., 1994). In the AFM experiment, the biotin molecules were fixed through linker molecules to the cantilever tip, and complexed with streptavidin tetramers. The tip was then brought into contact with an agarose bead to which biotin molecules were complexed, allowing cross-complexes to be formed. Upon subsequent retraction of the cantilever, biotin molecules were pulled out of their streptavidin pockets, and single rupture forces could be measured. In the parallel computer experiment (Grubmüller et al., 1996), the elastic cantilever was modeled as a harmonic spring, attached to

the biotin molecule at that position, where in the real experiment the linker molecule was connected. Simulations at different rupture rates in the pico-to-nanosecond range indicated the entering of a friction-dominated regime [regime (4)], which could then be extrapolated toward slower pull rates, obtaining good agreement with the AFM result. At the highest pull rates the rupture force saturated, most likely due to effects described in regime (5).

Experiments on lipid-membrane bond rupture

Adhesion forces of lipids in membranes have thus far been measured both by SFA experiments (Leckband et al., 1994, 1995), and by the BFP technique (Evans et al., 1991, 1995; Ludwig, 1996).

With the BFP technique, individual lipid-membrane bonds can be ruptured. The BFP experimental setup consists of a pipette-adhesed vesicle containing lipid-anchored avidin; the avidin is bridged to a biotin molecule, which is anchored to a functionalized bead. Single cross-complexes can be formed when the concentration of lipid-anchored avidin is low. Upon retraction of the vesicle-holding pipette, the lipid anchor is extracted out of the membrane. The rupture force can be calculated from measurement of the pressure fluctuation in the pipette. For distearoylphosphatidylethanolamine (DSPE) lipids extracted out of a stearoyloleoylphosphatidylcholine (SOPC) vesicle, the reported rupture force is 30 pN (Ludwig, 1996). A somewhat higher force of 41 pN is obtained in the same study extracting DSPE out of distearoylphosphatidylcholine (DSPC) vesicles containing 40 mol% cholesterol. The difference between the two measurements was statistically significant. The authors suggest it is caused by a strong interaction between the DSPE lipids and cholesterol on the one hand, and the presence of double bonds in the SOPC membrane on the other, making it more difficult for the DSPE lipid to be extracted out of the cholesterol-containing membrane.

The SFA experimental setup consists of two cylindrically curved plates covered with a biotinylated membrane surface. (The individual lipids are biotinylated at their headgroups, using a small spacer.) Adding streptavidin, cross-complexes are formed between the two plates if they are brought into close contact. When the plates are subsequently separated, patches of lipid molecules are extracted from each of the two cylinders, i.e., multiple bond breaking is observed. The maximum adhesion energy required to break the two surfaces apart can thus be obtained. For dipalmitoylphosphatidylcholine (DPPC) membranes, the measured adhesion energy of a DPPC molecule is 90–110 kJ/mol (Leckband et al., 1995). The authors calculated the rupture force of the lipid-membrane complex to be ~70 pN, assuming a bond length of 2.0 nm and a constant adhesion force along the unbinding path.

Compared to the value obtained by the BFP method, however, the SFA value should be considered as a lower limit, for two reasons. First, a nonconstant adhesion force along the unbinding path will result in a higher value of the rupture force compared to the value obtained with the assumption of a constant force. Second, as whole patches of lipids are extracted simultaneously, the measured adhesion energy corresponds to the maximum of the patch-averaged adhesion energy. Now, if a distribution of bond lengths exists for individual lipid molecules, which is a natural assumption under nonequilibrium conditions, the maximum of the mean adhesion energy is always lower than the mean of the maximum adhesion energies of individual lipid molecules. The latter value would result from averaging over many independent rupture experiments of single complexes, as in the case of the BFP method and also in the method we use (see below).

Taking the above considerations into account, the difference between the SFA and the BFP values is at least a factor of two, and possibly more, which should be attributed to the time scale difference of both methods. Whereas the BFP experiment most likely takes place in regime (2), where the thermal component induces diffusive motions of the lipids that lower the adhesion force, the SFA measurement is likely to be shifted toward regime (3), where the time scale becomes too short to probe significant diffusive motion.

METHODS

Membrane simulation

Since already various membrane models exist in literature (for a recent review, see Tieleman et al., 1997), we did not invent a new one but chose the force field and simulation parameters that have been published recently by Berger et al. (1997) for a DPPC membrane at full hydration. These authors noted that in actually all published lipid simulations of the liquid-crystalline phase that use united atoms, the density of the membrane is too low. Experimentally, the density of the membrane can—in contrast to the area/lipid—be accurately measured, and therefore provides a good basis for judging the validity of the force field. In order to obtain a better density, Berger et al. optimized the hydrocarbon Lennard-Jones (LJ) parameters of the OPLS force field (Jorgensen and Tirado-Rives, 1988) to obtain the correct density and enthalpy for pentadecane. In the membrane system, these optimized LJ parameters were used together with the GROMOS parameter set for angles and dihedrals (Egberts et al., 1994). Together with fractional charges derived by Chiu et al. (1995) the simulated DPPC membrane indeed showed a higher density, in good agreement with the experimental results. Other properties, such as the order parameter or atom distributions, gave good agreement with the experimental results for DPPC membranes in the lipid-crystalline phase as well (Berger et al., 1997).

We used the same simulation conditions as Berger et al.: the system is coupled to a constant temperature (323 K, $\tau = 0.1$ ps) and pressure bath (1 atm, $\tau = 1.0$ ps) (Berendsen et al., 1984). Due to the application of periodic boundary conditions, actually an infinite multilamellar system is generated. By constraining the bondlengths (SHAKE algorithm; Ryckaert et al., 1977), a time step of 2 fs could be used. LJ and electrostatic interactions were calculated at every time step within a sphere of 1.0 nm radius; electrostatic interactions were calculated up to 1.8 nm, and kept constant over a period of 10 time steps (twin range method). For more details about the force field and simulation parameters we refer to the original publication (model III; Berger et al., 1997).

In the simulations that we describe in this paper, the membrane system consists of 64 DPPC lipids, arranged in a bilayer conformation, and 3846 water molecules forming a large water layer (~5 nm). The inclusion of such a large water layer was necessary in order to pull individual lipids completely out of the membrane, without the problem that these lipids

interact with the periodic image of the other half of the bilayer. Such a large water layer is not stable in multilamellar systems; above the swelling limit (29.1 water molecules per lipid; Nagle et al., 1996), additional water forms a separate phase. In our system (60 waters/lipid), however, the excess water has no possibility to form a separate phase. The water layer is so large that no direct interactions between opposing lipids are computed, and also indirect interactions across such a large water layer are expected to be negligible. Therefore, effectively we simulate a monolamellar system, i.e., a single free membrane.

As recommended by various authors (van Buuren et al., 1993; Tieleman and Berendsen, 1996), and also used in the simulation of Berger, the water is modeled as simple point charges (SPC; Berendsen et al., 1981) and not the extended model SPC/E. Although the latter model performs better considering some structural and dynamical quantities, the thermodynamic potential of the original SPC model is much better. This property is important in interface studies, and even more so in the current experiments where the solvation of lipids is explicitly simulated.

As a starting structure for our simulations, we used the last time frame of the trajectory generated by Berger et al., which has a length of 500 ps and can be considered well-equilibrated (Berger et al., 1997). In order to increase the width of the water layer necessary for our experiments, we inserted a number of preequilibrated boxes of SPC water into our system. After energy minimization, the newly formed system was equilibrated for another 50 ps, long enough for the cell dimensions to attain their new equilibrium values (since mainly the water layer had to readjust itself, the required equilibration time remained short). Our system has an equilibrium area of 19.6 nm^2, and a mean perpendicular dimension of 10.2 nm. These values imply an area/lipid of 0.61 nm^2 and a volume/lipid of 1.24 nm^3, taking a constant volume for SPC water (1.03 g cm^{-3} at 323 K). Compared to the original system with less water of Berger et al., both the area/lipid and the volume/lipid have not changed significantly. Note that the application of NPT conditions allows the lipid membrane to adjust itself to the changing surface density during the extraction process. In Fig. 1 a snapshot of the membrane system is shown, in which already two lipids are extracted halfway out of the membrane by the method described below.

Lipid extraction

For each simulation, two lipids are pulled out simultaneously, from opposite sites of the membrane. By this procedure, two (quasi-) independent data sets are obtained from each simulation. The lipids are selected in such a way that their mutual distance is as large as possible. Thus, even when they are both completely pulled out (solvated in the water layer) their mutual distance is beyond the cutoff, implying no direct interaction.

In order to pull the selected lipids out of the membrane, they are simply attached to a harmonic spring:

$$V_{\text{spring}}(t) = 0.5\, K[z_{\text{link}}(t) - z_{\text{spring}}(t)]^2 \tag{5}$$

where V_{spring} is the harmonic spring potential, K the force constant, $z_{\text{link}}(t)$ the position of the atom to which the spring is linked, and $z_{\text{spring}}(t)$ the position of the spring. Moving the spring with constant velocity v_{rup} away from the membrane, the lipid is extracted out of the membrane:

$$z_{\text{spring}}(t) = z_{\text{spring}}(0) + v_{\text{rup}}\, t \tag{6}$$

In order to prevent the whole bilayer from being pulled away, the bilayer center of mass was kept in place. The required adhesion force is proportional to the deflection of the spring during the pulling process:

$$F_{\text{adh}}(t) = K\{z_{\text{spring}}(t) - z_{\text{link}}(t)\} \tag{7}$$

The distance $z_{\text{link}}(t) - z_{\text{P}}$ between the atom at which the spring is attached and the average position of the phosphorous atoms in the interface is chosen as the reaction coordinate R. The drawing in Fig. 2 gives an impression of the applied method.

The chosen setup is an idealization of the way in which lipids are pulled out by the existing experimental methods. In these methods the lipids are typically pulled out of the membrane via an array of lipid complexed molecules that are bridging the lipid to a surface that is being retracted at a certain pull rate. The harmonic spring in our method in fact mimics the response of this whole array of lipid-complexed molecules and the retracting surface itself as well. The position at which the harmonic spring is attached, one of the methyl groups of the choline headgroup, corresponds to the position where, experimentally, a linker molecule is attached.

As a force constant we used the same one as Grubmüller et al. (1996): $K = 2.8$ Nm^{-1} in their MD simulation of biotin-streptavidin rupture. This was chosen because it allows small, thermal fluctuations of the attached molecule. A larger force constant would restrain these thermal motions too much, whereas a smaller one would filter out the high-frequency components of the adhesion force. We refer to the Discussion section for possible consequences of the chosen force constant. Comparing our force constant to experimental setups is difficult, as the harmonic spring is an idealization of the experimental response. The response of the experimental setups usually consists of a combination of a response due to the apparatus itself, plus the contribution of an array of molecules complexed to the individual lipids, making it anharmonic. Due to the large masses involved, it is clear that the response of the experimental setups is much slower. Therefore, the experimental methods are unable to record the fluctuations on the nano-

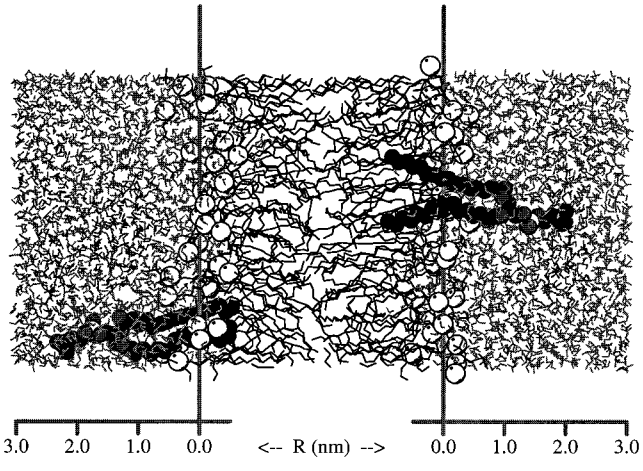

FIGURE 1 Snapshot of the lipid membrane in which two lipids are pulled out. The interfacial lines, P-planes, are drawn for reference, and represent the average position of the phosphorous atoms (*white spheres*). The snapshot is taken from a simulation at medium pull rate.

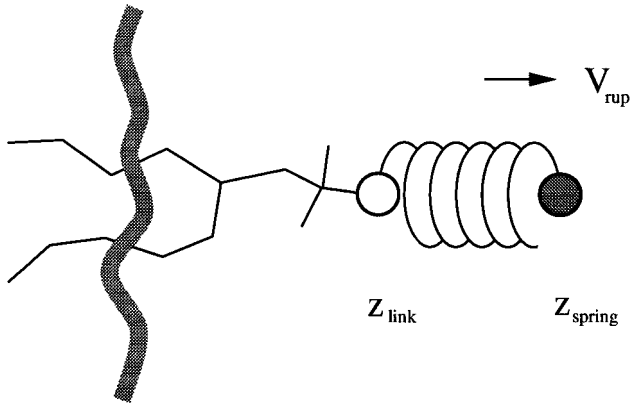

FIGURE 2 Schematic picture of the method that is used to extract the lipids. A harmonic spring is linked to one of the lipid methyl groups and moved away with constant velocity during the simulation.

second time scale and are (currently) limited to time scales beyond the millisecond range.

In order to pull the lipids completely out of the membrane (i.e., until complete dissolvation), a distance of ~4.0 nm has to be bridged. The initial position of the spring coincides with the position of the linked atom, i.e., $z_{spring}(0) = z_{link}(0)$. Although the required pull distance actually depends on the initial position within the bilayer of the selected lipid, 4.0 nm turned out to be sufficient in any case. A distance of 4.0 nm implies that the lipid crosses the midplane of the water layer. Due to the periodic boundary conditions it will then reappear on the other side. However, the water layer is large enough to assure that the distance between the end position of the extracted lipid and the other half of the bilayer is still much larger than the cutoff. Hence, the approach of the lipid toward the bilayer from the opposite site at the end of the extraction run is not expected to have a large influence.

To get information on the dependency of the adhesion forces on the pulling rate, we have performed simulations at seven different velocities (see Table 1).

At the highest pull rate, 0.05 nm/ps, a simulation of only 80 ps is needed to probe the full reaction coordinate of 4.0 nm. At the lowest pull rate, 0.001 nm/ps, 4 ns are required, the limit of our computational possibilities. In order to study an even lower pull rate, we therefore decided to only partially extract the lipids in the case with $v_{pull} = 0.0002$ nm/ps. The part of the path we chose to simulate in these cases was centered around the position at which in the next-slowest run the force maximum was observed (see Results). The width of the path was chosen as 0.8 nm, so the total simulation time needed in this case was 4 ns. Since we are dealing with nonequilibrium processes, the computed force profiles of individual lipid molecules may scatter considerably, even when extracted at the same velocity. Different lipids will take different, irreversible paths across the energy landscape. The simulations with high velocities showed a large scatter, and have been performed more than once, using different lipids (see Table 1). Note that every single simulation yields two independent force profiles, as we pull out lipids at both sides of the bilayer simultaneously. From the independent force profiles (i.e., two in the case of the lowest extraction rates, six in the case of the highest), a statistical error is obtained. The simulations up to 800 ps have been performed with the GROMOS simulation program (van Gunsteren and Berendsen, 1987) on various single-cpu workstations, at an average speed of 0.5 ps/cpu hour. The nanosecond simulations were run with GROMACS (van der Spoel et al., 1996) on a parallel machine developed at the Groningen laboratory. In this case, the average simulation speed was about a factor of 20 larger.

Data processing

For a number of reasons, we processed the computed force profiles through application of two different Gaussian filters. The first type of filtering, time filtering, was applied to filter out fast frequencies arising from random thermal motion as well as the resonance frequency of the pulling spring. The resonance frequency of the spring was measured from the decay of the position autocorrelation function of the headgroup atom to which the spring was attached. Almost independent of pull rate, this frequency was observed to be 5 ps. In order to remove the spring artefact, our force profiles were therefore smoothed with a Gaussian filter of 5 ps halfwidth. [In their simulation of rupture forces, using the same force constant, Grubmüller et al. (1996) used a Gaussian filter with a halfwidth of 4 ps in order to remove the resonances.] Application of the filter also removes the high-frequency components which are mainly due to random thermal motion. Because experimental methods are not sensitive enough to record these thermal fluctuations it is desirable to extrapolate rupture forces without these thermal fluctuations in order to compare them to experimental results. Beyond the 5 ps time scale the local force maxima arise from structural changes, i.e., breaking of hydrogen bonds or *trans/gauche* isomerization of the lipid tails.

A second set of data was obtained by applying a Gaussian filter based on distance rather than time. This filter was used in order to reduce the fluctuations in the thermodynamic force. These type of fluctuations arise from the fact that different lipids will sample different parts of the configuration space, since the experiments are performed at nonequilibrium conditions. Ideally one would sample many lipids and average them in order to get rid of these types of fluctuations. As we were only able to sample the adhesion forces of a few lipids per pull rate (6 at the highest, 2 at the lowest rates), the average force profiles will still contain a lot of statistical noise due to specific pathways followed by the lipids. If one assumes that the adhesion force is approximately constant over a certain distance, one can reduce the thermodynamic noise by averaging the profile locally. The width of the filter should be as large as possible in order to increase the accuracy of the average, but as small as possible to reflect the true adhesion force at the specific position along the reaction coordinate. We chose a halfwidth of 0.25 nm for the distance filter. (This implies that for the fastest pull rate, 0.05 nm/ps, the time filter equals the distance filter).

The way in which the independent force profiles are averaged should be carefully considered too. One could either average the profiles first, and then determine the point of rupture, or one could determine individual rupture points, and perform averaging afterward. The latter approach ("individual averaging") corresponds to an AFM or a BFP experiment, in which averages are obtained from individual rupture events, whereas the first approach ("ensemble averaging") resembles an SFA experiment in which many lipids are extracted simultaneously and only an average response of the whole ensemble is measured. Since our data are thought to be relevant to both methods, we compare both types of averaging.

Combining the two types of filtering (time and distance) with three types of averaging (none, individual, and ensemble) we generated six different data sets. From the six different force profiles, six different rupture points are obtained as well. The most accurate value of the rupture point that can be related to the SFA measurements will be obtained after both explicit averaging over different lipids, and implicit averaging using the distance filter. Individual averaging, on the other hand, relates to the BFP measurements, but one should take care using the distance filter in that case, as it implicitly averages over many lipid conformations. The different methods of averaging and filtering plus the relevance of the obtained rupture points are summarized in Table 2.

TABLE 1 Overview of performed simulations

Class	Pull Rate (nm/ps)	Number of Simulations	Time per Simulation	Symbol
Fast	0.05	3	80 ps	Circle
Fast	0.02	2	200 ps	Circle
Medium	0.01	2	400 ps	Diamond
Medium	0.005	2	800 ps	Diamond
Slow	0.002	2	2 ns	Triangle
Slow	0.001	1	4 ns	Triangle
Slow	0.0002	1	4 ns	Triangle

The class name is used in the text for general reference to simulations using similar pull rates. The symbols correspond to the type of symbols used in the figures (when appropriate).

TABLE 2 Overview of filtering and averaging methods

Filter	Averaging	Rupture Point	Compare to	Symbol
Time	None	F_{max}	*BFP*	White
Time	Individual	$\langle F_{max} \rangle$	$\langle BFP \rangle$	Black
Time	Ensemble	$\langle F \rangle_{max}$	$\langle SFA \rangle$	Gray
Distance	None	$[F]_{max}$	$\langle SFA \rangle$	White
Distance	Individual	$\langle [F]_{max} \rangle$	$\sim\langle BFP \rangle$	Black
Distance	Ensemble	$\langle [F] \rangle_{max}$	$\langle SFA \rangle$	Gray

The angle brackets denote averages over different lipids, the square brackets denote implicit averaging due to application of the distance filter. The *SFA* experiment automatically averages over many lipids. The symbols refer to the symbols used in the figures (when appropriate).

RESULTS

This section describes the response of the membrane to extraction of lipid molecules, the conformational changes of the extracted lipids, the measured adhesion force profiles, and the adhesion energy.

Membrane response

In Fig. 1 a snapshot of the membrane system is shown, with two lipids pulled out approximately halfway. It can be seen that the lipids are pulled out individually, i.e., no neighboring lipid molecules are simultaneously extracted, not even partially. We observed this in all simulations, both at the highest and at the lowest pulling rates. Apparently, the microscopic elasticity of the bilayer is rather low, and the membrane behaves like a fluid. This is also true for the membrane interior. The free volume that is created when the lipid is pulled out is almost immediately occupied by adjacent lipid molecules. Looking at the figure, it is clear that no hole is created in the membrane.

As a concomitant result of the changing surface density during the extraction process, the surface area of the membrane changed during the extraction of the lipids. The equilibrium area for the membrane with two fully extracted lipid molecules turned out to be 19.1 nm^2, compared to the initial value of 19.6 nm^2. The area/headgroup remains unchanged (0.61 nm^2), now with 31 lipids forming a monolayer instead of 32.

Conformational changes

In Fig. 3 a series of snapshots is shown, comparing the conformations of lipids during the extraction process at high and slow pull rates.

The first noticeable feature is that the lipids tend to attain a stretched conformation when they are extracted, which can be expected as the lipid experiences the least resistance from the surrounding lipids in a fully stretched conformation. There is no clear difference between the fast and slow extraction rates in reaching a stretched lipid conformation. It seems that in order to leave the membrane the lipid has no freedom to adopt a conformation deviating from fully stretched, even at the fastest rate. At slow pull rates the lipid partly folds when it is completely extracted, in contrast to high pull rates where the lipid maintains its stretched conformation. A folded conformation is energetically more favorable because it minimizes the area of water-exposed methyl groups. However, in the case of an applied pulling force, the friction forces make a streamlined conformation more favorable. The higher the pull rate, the larger the friction forces. The same arguments explain the difference between the P-N dipole vector, which is clearly more stretched in the high pull rate limit.

In Fig. 4 the conformational changes are further illustrated by showing the shift in the average number of *gauche* angles in the lipid tails during the extraction process at high, medium, and low speed.

In their equilibrium position within the membrane, an average number of 4.1 *gauche* angles pro tail is observed, in accordance with experimental results that indicate a range of ~4 *gauche* angles pro tail in the liquid-crystalline phase (e.g., Seelig and Seelig, 1980; Mendelsohn et al., 1989; Pink et al., 1980). Until the point where the lipid tail groups get dissolved, $R \simeq 2.5$ nm, the differences between conformations taken at different pull rates are only minor. A general drop of the number of *gauche* angles, almost by a factor of two, occurs along the unbinding path. At slow rates, the drop seems to take place a little faster, reflecting the increased sampling possibilities to obtain the stretched conformation required to leave the membrane. At the end, when the lipids are fully dissolved, the conformations depend strongly on the rate of pulling. In the high pulling rate limit, the lipid adopts a gel phase-like conformation, i.e., almost fully stretched. However, in the low pulling limit the number of *gauche* angles increases again in order to minimize water contact with the hydrophobic tails. The standard de-

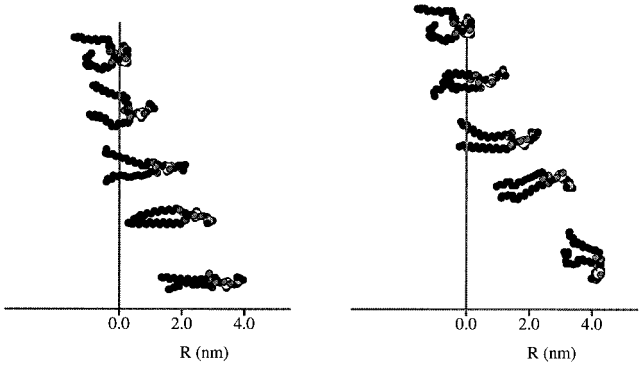

FIGURE 3 Subsequent snapshots of typical lipid conformations during the extraction process. *Left*: high pulling velocity; *Right*: low pulling velocity. The bold line corresponds to the P-plane (see Fig. 1).

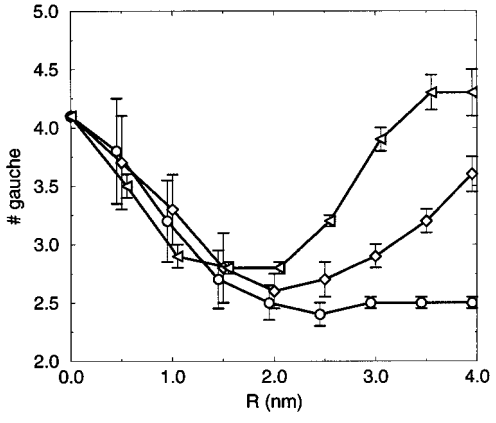

FIGURE 4 Average fraction of *gauche* angles (per lipid tail) during the extraction process. Circles, diamonds, and triangles are used for fast, medium, and slow pull rates, respectively (see Table 1). The bars indicate standard deviations obtained from comparing distance-averaged data of individual lipids in each of the three pull rate classes.

viations drawn serve as an indication of the different pathways taken by different lipids; the larger the bars the larger the spread in observed, locally averaged, conformations. Within the membrane, the largest spread in conformations is observed at fast pull rates. At low pull rates, the average pathways taken by individual lipids turn out to be very similar. After rupture, the sampled phase space at fast rates becomes very narrow; all lipids tend to be almost fully stretched.

Separate analysis of the conformational changes in the beginning, mid, and end of the lipid tails reveals that the *gauche* angles in the headgroup region undergo conformational changes first, followed by the *gauche* angles of the middle parts and finally of the endgroups. During the full extraction process almost all lipids retain at least one *gauche* angle (per lipid) near the headgroup, necessary for the lateral spacing of the two tails. Separate analysis of the headgroup dihedrals further shows that in all cases the stretching of the P-N dipole vector occurs in an early stage of the extraction process. Whereas the equilibrium angle between the P-N vector and the membrane plane is close to planar, upon retraction the angle stretches to close to perpendicular, in almost all cases within the first 0.5 nm of extraction. Only in the case of slow pulling rates does the angle adapt a wide range of other conformations once the lipid resides in the water layer completely.

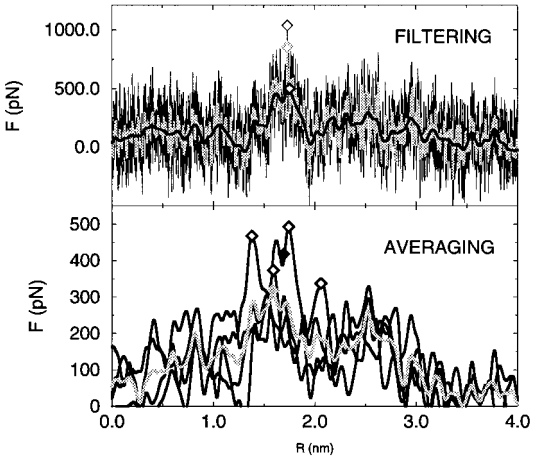

FIGURE 5 Illustration of the applied filtering and averaging methods. *Upper graph*: filtering. The thin black line denotes the original signal, the gray line after time filtering, and the thick black line after distance filtering. The open symbols denote the filter-dependent positions of the rupture event. *Lower graph*: averaging. Black lines denote individual, distance-averaged force profiles. The gray line is the ensemble average of the four individual profiles. The open symbols denote the scattered individual rupture points. The gray symbol represents the ensemble-averaged point of rupture, and the black symbol represents the individually averaged point of rupture (see Table 2).

Adhesion forces

In Fig. 5 we plotted an example of a recorded force profile in order to illustrate the methods of filtering and averaging that we used.

The upper graph shows the unprocessed force profile plus the same data smoothed with a Gaussian filter of both 5 ps and 0.25 nm halfwidth. The unprocessed data show a lot of noise due to fast thermal fluctuations, exaggerated by the artificial resonance of the spring. Not much insight is obtained from these data. The time filtering is performed to remove these fast thermal fluctuations. (We could have chosen a less sensitive spring to begin with, but it is more convenient to perform filtering afterward once the amount of useful information in the signal can be assessed more precisely.) Peaks in the time-filtered profile thus measure conformational changes over ~10 ps. The largest local peaks arise predominantly from the conformational changes in the lipid tails, i.e., from isomerization of the tail angles. The smaller maxima are mainly caused by the redistribution of (water-mediated) hydrogen bonds between the extracted lipid and its surrounding lipids. The distance filtering is applied to remove the fluctuations in the thermodynamic force (Eq. 1). In this case the observed peaks indicate more generally the state of the extracted lipids. Instead of individual hydrogen bond breaking or isomerization events, the force maxima arise from the total energy it costs the lipid to sustain its position. Apart from conformational contributions, nonbonded forces (electrostatic, van der Waals) as well as friction forces determine the position and height of the maxima.

The lower graph of Fig. 5 shows how different methods of averaging the data affect the magnitude of rupture forces and bond lengths. The ensemble-averaged point of rupture is obtained by first averaging the individual force profiles, and then locating the global maximum. The individually averaged point of rupture is obtained by averaging the individual points of rupture. The first method resembles the SFA approach, whereas the second method corresponds more closely to a BFP measurement. The figure shows that the ensemble-averaged rupture force is significantly lower than the individually averaged value, a generally observed feature in all of our simulations. It also shows that the point of rupture depends on the method of averaging as well, thus bond lengths deduced from SFA- and BFP-type measurements need not necessarily be the same.

To illustrate the generally observed shape of the adhesion force profiles as a function of pull rate, in Fig. 6 we compare the ensemble-averaged force profiles obtained after distance filtering.

From Fig. 6 it can be seen that the averaged forces are much higher at fast pull rates compared to slow pull rates. Basically, two effects account for this observation. The first effect is due to the nonequilibrium nature of this experiment. The extracted lipid has no possibility to extensively search for the least resistant path across the energy landscape. As the pull rate drops, the search time increases, and the crossing of large barriers can be avoided. Second, the frictious forces arising from the collisions with surrounding molecules decrease at lower pull rates. The general shape of

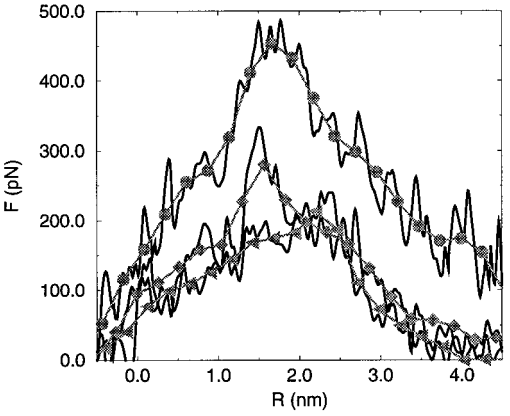

FIGURE 6 Ensemble-averaged force profiles with distance filter. The marked gray lines show the general shape of the curves. *Circles*: fast pull rate; *diamonds*: medium pull rate; *triangles*: low pull rate.

the force profiles is that of a triangle. The adhesion force gradually builds up toward its maximum value, after which it decreases again as the lipid has left the bilayer (compare x axis with Fig. 3).

The position and height of the largest force maximum, the rupture point, appears to depend on the pull rate. As we argued before, it also depends on the method of both filtering and averaging. Therefore, in Fig. 7 we present a scatter plot with all rupture points determined using the different methods described above.

The left graph shows the rupture points that are obtained after application of the time filter. From this graph the nonequilibrium nature of the experiment is evident: a large scatter is observed in the individual points of rupture for different lipids, both in the bond lengths and in the rupture forces. At high pull rates, the scatter in the bond lengths is

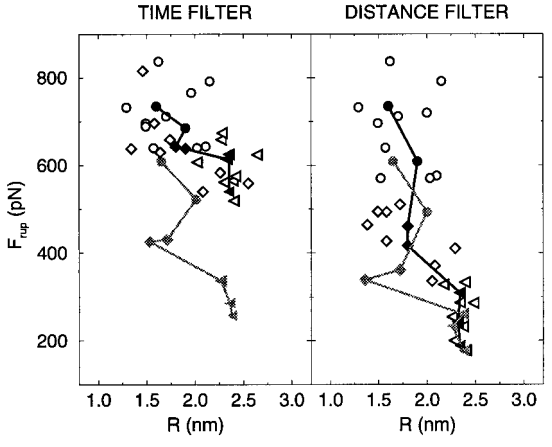

FIGURE 7 Scatterplot of the positions at which lipid-membrane rupture occurs against magnitude of the rupture force. *Left*: time-filtered data. *Right*: distance-filtered data. Open symbols represent individual rupture points, black symbols individually averaged ones, and gray symbols ensemble-averaged ones (see Table 2). Solid lines connect the averaged rupture points in order of decreasing pull rate. Circles, diamonds, and triangles are used for fast, medium, and slow pull rates, respectively (see Table 1).

almost 1.0 nm. Whereas some lipids experience maximum resistance after only 1.25 nm of extraction, other lipids follow a pathway with highest resistance only after >2 nm of extraction. At lower pull rates, the scatter has diminished, a result of the more uniform extraction pathways. The scatter in the maximum observed forces does not seem to decrease much, if at all. The observed rupture forces vary typically over a range of 200 pN within one class of pull rates. However, one should bear in mind that the slower the pull rate, the longer the sampling time around the point of rupture. A longer time implies more chance of finding a less resistive path out of the membrane, but also a higher chance of sampling unfavorable parts of configuration space. Thus, recalling Eq. 1, although the expectation values of the thermodynamic and friction forces decrease, the expectation value of the random force will increase with sampling time. Therefore, we assume that the large scatter of the rupture forces even at low pull rates originates from the increased random contributions.

Concentrating on the averaged rupture points, we see that the ensemble-averaged values are much lower than the individually averaged ones. As discussed before, ensemble averaging results in a reduction of noise present in the individual profiles. With both methods, we see that there is a clear shift in the average bond length upon decreasing pull rate, from $R \sim 1.7$ nm toward $R \sim 2.3$ nm. The latter value implies that rupture occurs at a position where the lipid is already pulled out for the largest part (compare Fig. 3). Apparently the forced withdrawal of the tail ends out of the hydrophobic membrane environment requires the largest force. This observation can be rationalized if one realizes that the endgroups of the lipid tails in our simulation possess the highest fraction of *gauche* angles, in agreement with experimental observation (Mendelsohn et al., 1989). At $R =$ 2.3 nm, the endgroups enter the membrane region with the highest density, the region of the glycerol linkage. A large entropic penalty can therefore be expected when the endgroups are pulled through this region. For the higher pull rates, the lipid molecule has no time to adjust its conformation fast enough, and will be more brutally forced in a stretched conformation. Therefore, the point of maximum resistance is expected to occur earlier in the extraction process.

The extraction processes observed at medium pull rates are a mixture between the dominant processes at either low or high pull rates. Fig. 7 shows that five lipids extracted at medium speeds fall into the class of high pull rates, and three more closely resemble those of low pull rates. The position and height of the ensemble-averaged point of rupture is therefore a bit misleading: the average is dominated by the lipids that follow pathways similar to those at high pull rates.

The distance filtered data (*right graph*) show essentially the same features as the time-filtered data. Due to the implicit averaging that is performed with the distance filtering, the noise in the data points is reduced and the features discussed above are more clearly visible. Especially

at low pull rates, the filtering of random noise results in a large decrease in the magnitude of the rupture forces. The individually and ensemble-averaged rupture points seem to converge, indicating that at these rates the lipids follow a pathway already very close to the equilibrium pathway. The (quasi-equilibrium) bond length can be determined quite accurately from these data, and is deduced to be $R = 2.35 \pm 0.1$ nm.

In order to compare the observed rupture forces to the experimentally determined values, we plotted the pull rate dependency of the rupture force in Fig. 8.

Two curves are shown: both are distance-filtered, the first is individually averaged, the second is ensemble-averaged. As discussed in the Methods section, the individually averaged rupture forces should be compared to BFP-like experiments, in which single lipids are extracted one at a time, and the ensemble-averaged data to SFA-like experiments, in which whole patches of lipids are extracted simultaneously. As noted earlier, both types of averaging seem to converge already on the time scale of MD. Toward the high pull rate limit the rupture force seems to saturate, most likely due to effects described in regime (5). We could expect a friction-dominated linear regime (4) as the pull rate drops, since as we already argued (Fig. 7) in this limit the pathways are likely to resemble the equilibrium pathways. Such a conclusion is, however, hard to draw from our data, as we have only three independent data points in this regime, only the last two of which really have converged.

The inserted graph in Fig. 8 shows the approach of the simulated data toward the experimental data. If one assumes that the difference of ~100 pN between the experimental SFA value and the slowest simulated value is mainly due to friction, one would estimate (Eq. 4) a local friction coefficient of $\xi(R_{rup}) = 50$ pN s m^{-1}, or a local diffusion constant of 0.7 10^{-6} cm^2 s^{-1}. Using this value, and Stokes' relation for a sphere $\xi = 6\pi r\eta$ (as an order of magnitude guess; using the corresponding equation for a cylinder hardly changes the result), the resulting local viscosity is $\eta = 0.007$ kg m^{-1} s^{-1} (with r chosen as the radius of a circle with an area equal to the area per lipid, 0.61 nm^2). This value is about an order of magnitude larger than that of bulk water. As the lipid is largely surrounded by water at the point of rupture, this simplistic argument implies either the water close to the membrane not to be bulk-like, or the viscosity of the lipid headgroups, to which the tails of the extracted lipid still adhere, to be of dominant influence.

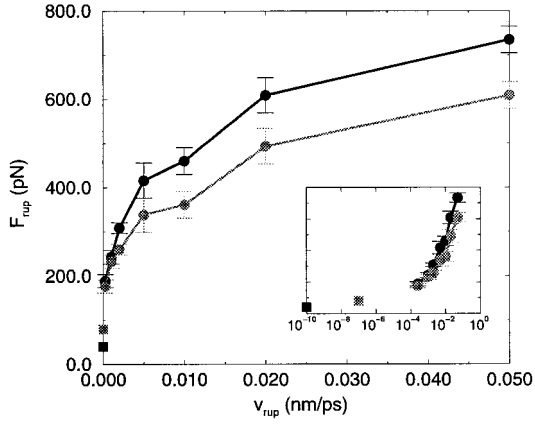

FIGURE 8 Plot of rupture force F_{rup} versus pull rate v_{rup}. Black circles correspond to individually averaged forces, gray circles to ensemble-averaged forces. The black and gray squares represent the experimental values from BFP (Ludwig, 1996), and SFA (Leckband et al., 1995) measurements, respectively. Note that on this scale the experimental pulling rate is virtually zero. The given error bars are statistical standard errors. Inset: same data on a logarithmic x axis to show the differences in pull rates between the experimental and simulated setups.

Adhesion energy

Another useful way of presenting the data is in the form of an adhesion energy, which is obtained from the adhesion force profile by simple integration (Eq. 2). Note that in this case the method of filtering is unimportant, as the integration procedure itself acts as a filter. In Fig. 9 the adhesion energy averaged over the slowest rates is presented.

The increase in adhesion energy is nonlinear with the largest slope at the point of rupture. The energy required to move the lipid further away from the rupture point is much less, but still not negligible at this rate. The total adhesion energy adds up to over 300 kJ/mol. Comparison of this energy with the estimated free energy of at most 100 kJ/mol for similar lipids (Cevc and Marsh, 1987) leads to the conclusion that much of the work done to extract the lipids on the MD time scale is due to friction, provided the earlier conclusion that the followed pathways are close to equilibrium holds. The computation of the free energy profile itself is the topic of a separate study, currently in progress. Preliminary results indicate that the shape of the profile as presented in Fig. 9 remains essentially unchanged.

In Fig. 9 a hypothetical adhesion energy profile is given, which is based on the assumption of a constant adhesion

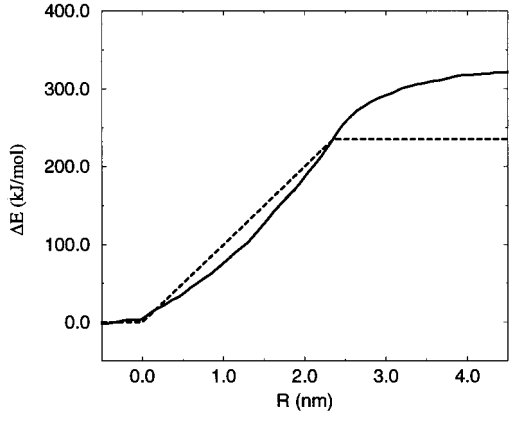

FIGURE 9 Adhesion energy profile. Solid line denotes the adhesion energy obtained from integration of the adhesion force profiles (averaged over all simulations with slow pull rates). Dotted curve shows a hypothetical profile in which a constant adhesion force is assumed up until the point of rupture.

force along the unbinding pathway. This assumption is usually made when interpreting SFA adhesion energies in terms of rupture forces. A rupture force estimated from the assumed profile will be significantly lower than the actually observed one.

DISCUSSION

Our results show that when lipids are pulled out at rates slower than ~0.005 nm/ps, a regime is entered where the individual extraction pathways converge to a single, general pathway. At the lowest pull rates, the lipid seems to have sufficient time to search for an energetically favorable conformation during the extraction process. The decrease in the magnitude of the rupture force in this regime is therefore expected to be predominantly due to a decrease in friction forces. At realistic pull rates (which are still at least 4 orders of magnitudes slower), the viscous forces will continue to decrease, but the conformational changes of the lipid during the extraction process will be essentially the same. (To obtain more insight into the preferred configurational states of lipids along the unbinding path, simulations under equilibrium conditions are currently underway.) Based on our results in the slow pulling regime, these conformational changes can be characterized as follows: as the lipid is dragged out of the membrane, it will adapt a conformation that is as linear as possible. After the initial stretching of the headgroup, the tails of the lipids undergo *trans/gauche* isomerizations, starting with the dihedrals closest to the headgroup, and ending with those near the tail ends. When the ends of the lipid tails are forced to enter the region of the membrane immediately behind the headgroups, a dense and highly ordered part of the membrane, the lipids feel a strong adhering force. This force is further enhanced through the increased exposure of the hydrophobic tails toward a polar environment. Once the tails are pulled out of lipid completely, the tails fold up rapidly in order to increase their entropy and minimize the contact with the surrounding water molecules. Consequently, the adhesion force decreases rapidly. The point of rupture thus occurs at a position at which the lipid is about to leave the membrane completely, between 2.2 and 2.5 nm away from its equilibrium position.

If we compare the rupture of the membrane-lipid bond to that of the biotin-streptavidin complex, simulated using a similar method by Grubmüller et al. (1996), we note the following important differences. In their simulations it turned out that the force profile was dominated by the making and breaking of directed hydrogen bonds. The strongest hydrogen bond, independent of pull rate, determined the point of rupture. Lacking strongly directional hydrogen bonds along the lipid extraction pathway, in our case the observed maxima in the force profiles are much more abundant and less pronounced [compare time-filtered profile of Fig. 5 with Fig. 3 *A* of Grubmüller et al., 1996]. Since the pathway of rupture seemed to be well preserved over a large range of studied pull rates, Grubmüller et al. were able to probe a friction-dominated regime [regime (4)] in which the rupture force varies linearly with rupture rate. In our case we might have just reached the onset of a friction-dominated regime, but simulations at even slower time scales would be required to test this hypothesis.

Interestingly, recent simulations of the unbinding of the biotin-streptavidin complex by Izrailev et al. (1997) fail to reproduce the linear regime observed by Grubmüller et al. The difference is attributed mainly to the differences in force fields. Using theoretical arguments, the same authors also show that, in the case of the biotin-streptavidin rupture, extrapolation of the MD data to the experimental AFM data should be done with care, as the AFM experiment most likely takes place in regime (2). In this regime, diffusion is important, lowering the required rupture force to unbind the complex. Similar considerations are likely to be valid in our case as well, making quantitative comparison to the experimental data difficult. Nevertheless, we feel that our simulated data have some direct consequences for the interpretation of the experimental data. The individual rupture events show some scatter, both in bond lengths as well as in rupture forces. At the lowest rates, the bond lengths vary roughly between 2.2 and 2.5 nm, and the forces have a standard deviation of ~25 pN. As a consequence, the ensemble average and the individually averaged rupture forces are not entirely equal, although rather close (Fig. 8). If the differences would converge further at the same rate, both types of averaging would be the same at the time scale of the experiments. However, BFP measurements (Ludwig, 1996) show that even at the millisecond time scale a significant amount of fluctuation in the measured rupture forces is present. For the extraction of DSPE out of SOPC membranes, the authors report a standard deviation of 14 pN compared to the mean value of 30 pN. Therefore, it seems likely that the scatter in rupture points will remain at a level not too far away from the level we observe. In that case, the estimated rupture force of an SFA measurement will always be an underestimation compared to the BFP experiment. Based on our results, an upper bound for this difference is 10 pN. Another MD result that has consequences for the interpretation of experimental results, in particular that of SFA, is the value of the bond length. In order to convert the adhesion energy measured by SFA to a rupture force, a bond length of typically 2.0 nm is assumed (Leckband et al., 1995). Our results show that, on average, rupture takes place over a somewhat larger distance of 2.35 nm. This would reduce the estimated value of the rupture force. However, our results indicate the first 0.3–0.4 nm of extraction merely cause a stretching of the headgroup; the position of the lipid tails remain unaffected. In the experimental setups, where large bulky groups are attached to the lipids that are pulled out, it is more likely that the initial equilibrium conformation will be one in which the headgroup is already fully stretched. If that is the case, a bond length of 2.0 nm seems quite accurate.

A more serious error in the interpretation of SFA data is expected when we consider a third result from our simulations: the adhesion force is not constant along the unbinding path. Assuming it to be constant results in an underestimation of the true rupture force. Fig. 6 shows that, as a first approximation, the rupture force increases linearly up to the point of rupture. Using this assumption (and assuming a bond length of 2.0 nm), we calculate a more realistic value of 140 pN for the rupture force in the case of the SFA experiment, i.e., double the value of the reported 70 pN (see also Fig. 9).

Finally, we want to briefly discuss the limitations of our results due to the explicit choices we made in modeling this lipid-membrane rupture process. Although we only studied a DPPC membrane, and although we have selected just one type of force field, we believe that the computed features are—at least qualitatively—applicable in related systems. For instance, the location of the rupture point, where the lipid is almost fully stretched and for the larger part surrounded by water, can be explained by some basic principles: entropy of chain stretching, excluded volume, and hydrophobic effect. These principles will be important in all realistic membrane systems, and are not mere artifacts of chosen simulation parameters.

Quantitatively, however, one might expect the results to change to some extent, depending on system and force field details. The treatment of long-range electrostatic interactions can be especially important. Ideally, one would like to use no cutoffs, and various methods exist to solve Poisson's equation for the whole system. One problem with these types of methods is, however, that they generate replicas of the system extended to infinity, thereby enhancing the effect of local fluctuations. Especially in our case, where we simulate in fact a very large fluctuation, the use of such methods seems inappropriate. Instead, we used an unusually large cutoff; as large as possible within the size of the system. Other methods, such as multipole expansion techniques, have not been tested in bilayers with periodic boundary conditions (Heller et al., 1993).

Another source of concern is the pressure coupling, which is required in order to let the system respond to the changing surface area. From the decay of the autocorrelation function of the surface area of a lipid membrane simulated under equilibrium conditions, it is deduced that long relaxation times are present, much longer than the pressure coupling time (1.0 ps), and independent of it. Actually, a whole hierarchy of relaxation times exist, ranging from picoseconds to nanoseconds. Therefore, one could expect that, comparing the time scales of fast and slow pull rates, the response of the membrane to the extraction of a lipid to be significantly different. Nevertheless, we observed that the membrane response looks similar. We therefore assume that the local reorganization of the membrane is governed by fast time scales, in the picosecond range. Note that the extraction of a lipid locally enhances the compressibility of the membrane, facilitating rapid reorganizations.

Apart from the force field details, results can be expected to depend on the choice of the force constant of the harmonic spring that was used to pull the lipids out of the membrane. Test runs with other spring constants showed that the time-filtered data are most sensitive. Upon reduction of the spring constant by a factor of four, for instance, the time-filtered rupture forces show a systematic decrease of ~50 pN. However, as soon as some kind of averaging is applied, either explicitly or through the application of the distance filter, results prove to be less sensitive to the value of the spring constant. The spring constant thus predominantly affects the magnitude of the fast fluctuations, not of the slower modes. In some model calculations, Izrailev et al. (1997) explicitly showed that the use of softer springs leads to the measuring of more global properties of the system. In that way the effect of a soft spring is mimicked by the averaging procedures we used.

CONCLUSIONS

The results of the simulations have provided us with some interesting insights into the way that lipids adhere in a lipid membrane. Although still far away from the time scales studied by experimental techniques and biologically relevant ones, features of the simulated lipid pull-out are likely to be relevant at slower time scales, too. Summarizing, the most important features, based on the slowest pull rates studied, are: 1) lipids leave the membrane without noticeable disruptions of the membrane structure; 2) during the pull-out, the lipids will adapt a gel-like conformation; 3) the adhesion force is strongest at the stage where the lipid is almost fully solvated; only the tail ends still adhere to the membrane; 4) a small but significant scatter is observed for the rupture forces of individually extracted lipids.

D.P.T. was supported by the European Union under Contract CT94-0124.

REFERENCES

Bell, G. 1978. Models for the specific adhesion of cells to cells. *Science.* 200:618–627.

Berendsen, H. J. C., J. P. M. Postma, W. F. van Gunsteren, A. DiNola, and J. R. Haak. 1984. Molecular dynamics with coupling to an external bath. *J. Chem. Phys.* 81:3684–3689.

Berendsen, H. J. C., J. P. M. Postma, W. F. van Gunsteren, and J. Hermans. 1981. Interaction models for water in relation to protein hydration. *In* Intermolecular Forces. B. Pullman, editor. D. Reidel Publishing Co., Dordrecht. 331–342.

Berger, O., O. Edholm, and F. Jähnig. 1997. Molecular dynamics simulations of a fluid bilayer of dipalmitoylphosphatidylcholine at full hydration, constant pressure, and constant temperature. *Biophys. J.* 72: 2002–2013.

Cevc, G. and D. Marsh. 1987. Phospholipid Bilayers: Physical Principles and Methods. John Wiley & Sons, New York.

Chiu, S. W., M. Clark, V. Balaji, S. Subramaniam, H. L. Scott, and E. Jakobsson. 1995. Incorporation of surface tension into molecular dynamics simulation of an interface: a fluid phase lipid bilayer membrane. *Biophys. J.* 69:1230–1245.

Egberts, E., S. Marrink, and H. Berendsen. 1994. Molecular dynamics simulation of a phospholipid membrane. *Eur. Biophys. J.* 22:423–436.

Evans, E., D. Berk, and A. Leung. 1991. Detachment of agglutinin-bonded red blood cells I. Forces to rupture molecular-point attachments. *Biophys. J.* 59:838–848.

Evans, E., and K. Ritchie. 1997. Dynamic strength of molecular adhesion bonds. *Biophys. J.* 72:1541–1555.

Evans, E., K. Ritchie, and R. Merkel. 1995. Sensitive force technique to probe molecular adhesion and structural linkages at biological interfaces. *Biophys. J.* 68:2580–2587.

Florin, E., V. Moy, and H. Gaub. 1994. Adhesion forces between individual ligand-receptor pairs. *Science.* 264:415–417.

Grubmüller, H., B. Heymann, and P. Tavan. 1996. Ligand binding: molecular mechanics calculation of the streptavidin-biotin rupture force. *Science.* 271:997–999.

Heller, H., M. Schaefer, and K. Schulten. 1993. Molecular dynamics simulations of a bilayer of 200 lipids in the gel and in the liquid-crystal phases. *J. Phys. Chem.* 97:8343–8360.

Izrailev, S., S. Stepaniants, M. Balsera, Y. Ono, and K. Schulten. 1997. Molecular dynamics study of unbinding of the avidin-biotin complex. *Biophys. J.* 72:1568–1581.

Jorgensen, W., and J. Tirado-Rives. 1988. The OPLS potential functions for proteins. Energy minimizations for crystals of cyclic peptides and crambin. *J. Am. Chem. Soc.* 110:1657–1666.

Leckband, D., W. Müller, F. Schmitt, and H. Ringsdorf. 1995. Molecular mechanisms determining the strength of receptor-mediated intermembrane adhesion. *Biophys. J.* 69:1162–1169.

Leckband, D., F. Schmitt, J. Israelachvili, and W. Knoll. 1994. Direct force measurements of specific and nonspecific protein interactions. *Biochemistry.* 33:4611–4624.

Ludwig, F. 1996. The Anchor Strength of Lipids in a Vesicle Membrane Studied by Force Spectroscopy. Ph.D. thesis. Technical University of Munich.

Mendelsohn, R., R. A. Davies, J. W. Brauner, H. F. Schuster, and R. A. Dluhy. 1989. Quantitative determination of conformational disorder in the acyl chains of phospholipid bilayers by infrared spectroscopy. *Biochemistry.* 28:8934–8939.

Nagle, J. F., R. Zhang, S. Tristram-Nagle, W. J. Sun, H. I. Petrache, and R. M. Suter. 1996. X-ray structure determination of fully hydrated L_α phase dipalmitoylphosphatidylcholine bilayers. *Biophys. J.* 70: 1419–1431.

Pink, D. A., T. J. Green, and D. Chapman. 1980. Raman scattering in bilayers of saturated phosphatidylcholines. Experiment and theory. *Biochemistry.* 19:349–356.

Ryckaert, J. P., G. Ciccotti, and H. J. C. Berendsen. 1977. Numerical integration of the cartesian equations of motion of a system with constraints: molecular dynamics of *n*-alkanes. *J. Comp. Phys.* 23: 327–331.

Seelig, J., and A. Seelig. 1980. Lipid conformation in model membranes and biological systems. *Q. Rev. Biophys.* 13:19–61.

Sefton, B., and J. Buss. 1987. The covalent modification of eukariotic proteins with lipids. *J. Cell. Biol.* 104:1449–1453.

Tieleman, D. P., and H. J. Berendsen. 1996. Molecular dynamics simulations of a fully hydrated dipalmitoylphosphatidylcholine bilayer with different macroscopic boundary conditions and parameters. *J. Chem. Phys.* 105:4871–4880.

Tieleman, D., S. Marrink, and H. Berendsen. 1997. A computer perspective of membranes: molecular dynamics studies of lipid bilayer systems. *Biochim. Biophys. Acta.* in press.

van Buuren, A., S. Marrink, and H. Berendsen. 1993. A molecular dynamics study of the decane/water interface. *J. Phys. Chem.* 97:9206–9212.

van der Spoel, D., A. R. van Buuren, E. Apol, P. J. Meulenhoff, D. P. Tieleman, A. L. T. M. Sijbers, R. van Drunen, and H. J. C. Berendsen. 1996. Gromacs User Manual version 1.2. Nijenborgh 4, 9747 AG Groningen, The Netherlands. Internet: http://rugmd0.chem.rug.nl/~gmx.

van Gunsteren, W. F., and H. J. C. Berendsen. 1987. GROMOS-87 Manual. BIOMOS BV Nijenborgh 4, 9747 AG Groningen, The Netherlands.

Woodle, M. C., and D. D. Lasic. 1992. Sterically stabilized liposomes. *Biochim. Biophys. Acta.* 1113:171–199.